An Optimal Genetic Algorithm for Fatigue Life Control of Medium Carbon Steel in Laser Hardening Process

Gennaro Salvatore Ponticelli [1,2,*] **, Stefano Guarino** [2] **and Oliviero Giannini** [2,*]

1   Department of Enterprise Engineering, University Tor Vergata, Via del Politecnico 1, 00133 Rome, Italy
2   Department of Engineering, University Niccolò Cusano, Via Don Carlo Gnocchi 3, 00166 Rome, Italy;
    stefano.guarino@unicusano.it
*   Correspondence: ponticelli@dii.uniroma2.it (G.S.P.); oliviero@unicusano.it (O.G.)

check for
updates

Featured Application: **The laser hardening process is suitable for extending the life of many engineering components, such as bearings, shafts and gears. The proposed genetic algorithm-optimized empirical model allows us to speed up the characterization of the process.**

Abstract: This study proposes a genetic algorithm-optimized model for the control of the fatigue life of AISI 1040 steel components after a high-power diode laser hardening process. First, the effect of the process parameters, i.e., laser power and scan speed, on the fatigue life of the components after the laser treatment was evaluated by using a rotating bending machine. Then, in light of the experimental findings, the optimization model was developed and tested in order to find the best regression model able to fit the experimental data in terms of the number of cycles until failure. The laser treatment was found to significantly increase the fatigue life of the irradiated samples, thus revealing its suitability for industrial applications. Finally, the application of the proposed genetic algorithm-based method led to the definition of an optimal regression model which was able to replicate the experimental trend very accurately, with a mean error of about 6%, which is comparable to the standard deviation associated with the process variability.

1. Introduction

The request for more precise processing operations for an improvement in the mechanical performances of structural components have made traditional manufacturing processes unsuitable for modern engineering. For this reason, innovative and advanced production processes have been introduced to address the needs of modern industry, especially when dealing with technological frontiers. In fact, one of the most important targets to achieve is the satisfaction of the stringent requirements of today's designers and producers in terms of the life of the parts [1,2]. In particular, many engineering components, such as bearings, shafts and gears, must resist the wearing phenomena with a hard surface and, at the same time, a tough inner core should guarantee the absorption of energy without fracture when subjected to high stress [3,4]. Such heterogeneous properties can be engineered by selectively hardening the surface using many different approaches, such as heat and mechanical treatments, alloying or coating the surface of the components, etc. However, these processes are often expensive and time consuming. Moreover, they usually do not allow for the selective treatment of small portions of the component. In light of this, lasers have appeared as an innovative and valuable solution for the thermal surface treatment of steel components thanks to their selectivity, ease of use and control,

which facilitates their manipulation [5–7]. In fact, lasers can provide localized surface heating. Part of this heat is transferred to the workpiece, leading to an increase in its surface temperature and resulting, therefore, in its austenitization. In fact, alternating heating and cooling phases very quickly on the surface can transform it into martensite, which is harder than the bulk material [8,9]. Moreover, with a laser, the heat input can be controlled very precisely and selectively on the surface of the components, due to the ability to accurately define the illuminated area, together with the short timescale of energy transfer into the material [10]. This ensures a reduced and localized deformation of the part, therefore limiting, and eliminating in the best case, any further post-processing operation [10,11]. However, it must be noted that there are two main sources of residual stresses during the heat treatments of steels: (i) stresses caused by the transformation of the austenite; (ii) thermal stresses caused by the different cooling rates and strain incompatibilities [12]. In particular, the resulting stresses are of the compressive type, which lead to the improved hardness of the surface [13]. In fact, the internal stresses are limited only to the depth at which the martensitic transition occurs, thus resulting in the limited distortion of the component.

Among the different laser systems available today, high-power diode lasers (HPDL) are particularly suited for the hardening treatments due to the rectangular or elliptical shape of the laser beam profile, which is able to ensure a uniform heating on large areas of the treated surface [14,15]. This is an essential requirement for the laser treatment to be effective [16]. In fact, typical industrial CO_2 lasers are not able to produce an energy flux into the stainless steel, and metals in general, high enough to promote the hardening process [17]. This is usually due to the reflection of the metal materials at the CO_2 wavelength. However, the application of a coating on the component to be heat treated can increase the absorptivity at the CO_2 wavelength [18]. But this introduces additional costs to the process both for its application and the subsequent removal. However, the use of high-power diode lasers avoids coating the surface of the workpiece because they produce wavelengths in which metals show greater absorptivity [17,19,20].

In thermal-based surface treatments, as it is for laser hardening, the main target is to achieve the requested mechanical performance, e.g., strength, hardness, wear resistance, etc., while minimizing thermal deformation. However, very often, these requirements are mutually exclusive and, therefore, the optimization of the process becomes a challenging task. In this context, the development of predictive models appears to be a virtual solution in order to reduce time and costs in finding the optimal operational process conditions. To this end, many research studies have focused on the development of relationships between process parameters and process responses [21–23]. Thus, research in laser hardening process development, optimization, modelling and simulation plays a critical role in advancing surface engineering science and technology [24].

In this light, the present work is aimed at proposing a genetic algorithm-optimized empirical model able to describe the fatigue behaviour in terms of the number of cycles until failure for different sets of process parameters for the laser hardening process of AISI 1040 medium carbon steel. The choice of such a material is due to its suitability for thermal hardening treatments and because it is commonly used in structural components as gears, shafts, axles, bolts, and so forth [25]. The experimental campaign [26] showed an overall improvement in the fatigue life of the components after the laser treatment, also exhibiting a significant dependence on the process parameters, i.e., laser power and scan speed. Moreover, the genetic algorithm-based regression model developed is able to replicate the experimental data very accurately, thus revealing its suitability for laser hardening process optimization.

2. Materials and Methods

The starting material is a commercial medium carbon steel (AISI 1040, [27]). The typical mechanical and thermal properties of the AISI 1040 steel are reported in Table 1, while the chemical composition is described in Table 2. Starting from 2 m bars, the geometry reported in Figure 1 was obtained by machining the samples using a milling machine with medium finishing inserts. The thermal treatments for surface hardening were performed using a 1.5 kW high-power diode laser (Rofin-Sinar model

DL015, Plymouth, UK), with a wavelength of 940 nm and an elliptical spot of 0.6 and 1.9 mm along the minor and major axes, respectively. During the laser treatments, the samples were held and rotated on a CNC turning device (DENFORD, Brighouse, West Yorkshire, UK), as reported in Figure 2. For protection and insulation purposes, a constant inert gas flow of 2.5 L/h of Argon was directed to the surface of the sample.

Table 1. Mechanical and thermal properties of AISI 1040 [27].

Property	Value(s)	Unit
Tensile strength	500	MPa
Yield strength	415	MPa
Young's Modulus	200	GPa
Poisson coefficient	0.3	-
Hardness Rockwell	13	-
Heat capacity *	486–770	J/kgK
Thermal conductivity *	30.1–50.7	W/mK

*: evaluated in the range 273–973 K. In particular, the thermal conductivity increases for decreasing temperature.

Table 2. Chemical composition of AISI 1040 [27].

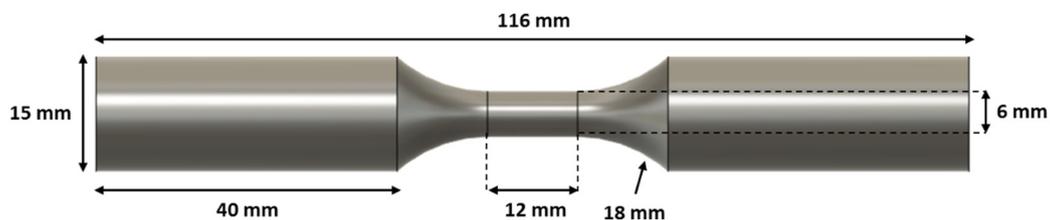| Element	Wt%
C	0.37–0.44
Mn	0.50–0.80
Si	0.15–0.40
P	≤0.035
S	≤0.035

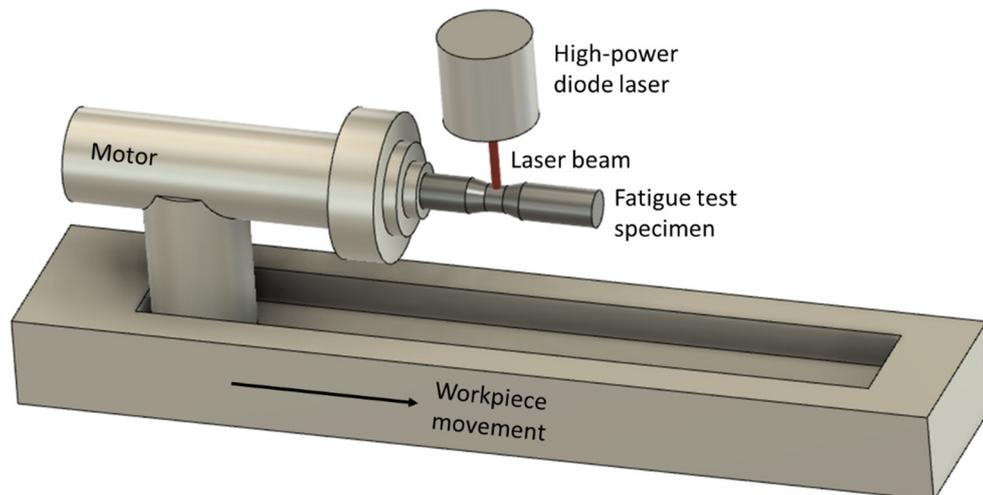**Figure 1.** Geometry of the samples obtained according to ASTM E466.

Figure 2. High-power diode laser system.

The experimental factors investigated were laser power (P) and scan speed (Ss), as reported in Table 3. In particular, the scan speed (i.e., peripheral speed) is calculated as the product between the rotational speed and the radius of the samples middle section.

Table 3. Experimental factors. 5 terms of $P \times 5$ terms of Ss = 25 experimental scenarios.

Factor	Values					Unit
Laser power (P)	100	150	200	250	300	W
Scan speed (Ss)	12	14	16	18	20	mm/s

The laser focus and the number of passes were fixed, respectively, at 0 and 1, because defocusing the laser beam and increasing the number of times that the laser passed on the treated area reduced the resulting hardness [19,28,29]. For each condition investigated, i.e., 5 terms of $P \times 5$ terms of Ss, the rotational speed and the beam feed were properly chosen to ensure no overlap in the laser scans during the thermal treatment, and therefore only one pass [29]. All the tests were replicated three times, with a total of 75 experimental tests. After that, a four-point rotating bending machine was used to carry out the fatigue tests (see Figure 3), in order to evaluate the number of cycles until failure (N). The samples were loaded with alternate cycles of tensile and compressive stresses as they were simultaneously bent and rotated. To this end, the untreated samples were tested in order to identify the value of the alternating stress to be adopted during the fatigue tests of the heat-treated samples so that a low-cycle fatigue behaviour was assured, i.e., within the range 10^4–10^5 cycles for steel materials [30,31]. Therefore, from the resulting Wöhler curve (see Figure 4), the alternating stress was set at a value of approximately 425 MPa, i.e., corresponding to a constant load F of about 120 N.
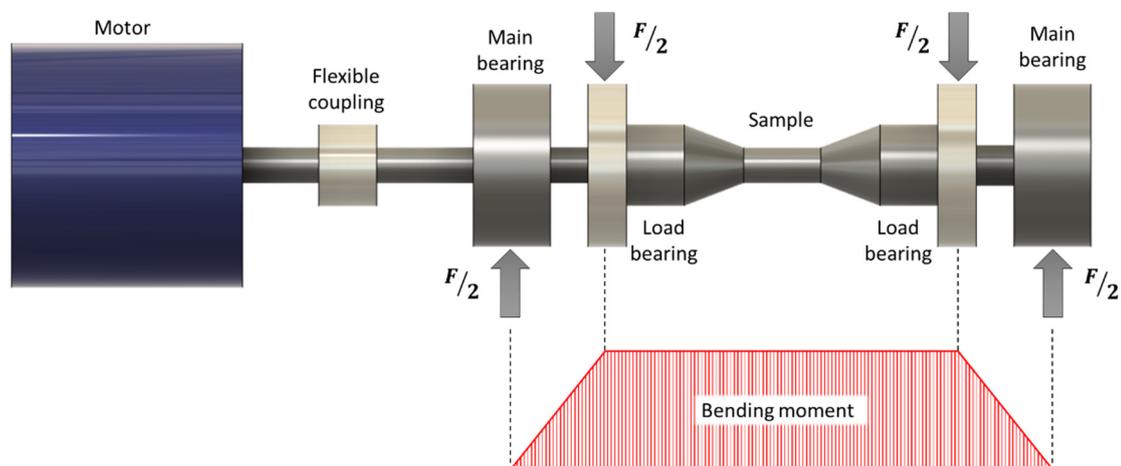
Figure 3. Schematic representation of the four-point rotating bending machine.
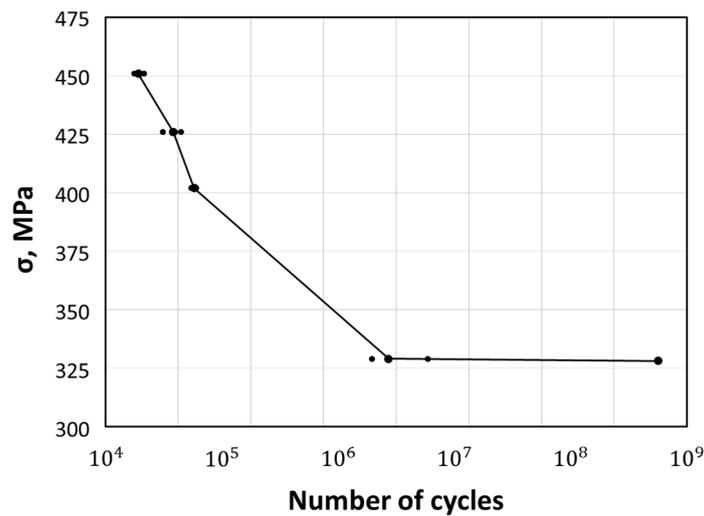
Figure 4. Wöhler curve for the untreated samples.

2.1. Computational Procedure

Manufacturers and researchers are interested in finding the best relationship between input(s) and output(s) with the aim of predicting and controlling the final quality of a process saving time and costs. This is usually accomplished by using empirical models. However, the choice of the best one is a challenging task that is not straightforward because of the very high number of possibilities, especially when dealing with data affected by dispersion due to both process and measurement variability. For this reason, in this work, a genetic algorithm (GA) is proposed and implemented in order to find the best empirical model (see Equation (1)) and, therefore, for the global optimization of the laser hardening process presented in this work in terms of the number of cycles until failure (N_{GA}). The choice of this evolutionary-based method is due to the ability to handle the optimization of many variables in a robust and efficient way [32–35].

$$N_{GA}(P, Ss) = k_0 + \sum_{i=1}^{N_T} \left(k_i \cdot P^{\alpha_i} \cdot Ss^{\beta_i} \right). \tag{1}$$

Given a defined number of terms N_T, Equation (2) represents a generic regression model in which α_i and β_i are optimized using the proposed GA, while the empirical coefficients k_i and the constant term k_0 are obtained with standard linear regression.

Figure 5 reports the procedure of the proposed algorithm as it is typically implemented: it consists of four steps, i.e., initialization, selection, crossover and mutation [36]. In this case, the crossover and mutation operators are used in parallel, in order to emphasize the gains in performance that can be achieved from the concurrent application of operators with different and complementary roles [37]. Furthermore, two other important concepts are the genetic encoding of the parameters and the formulation of the fitness function, which are explained in the following Figure.
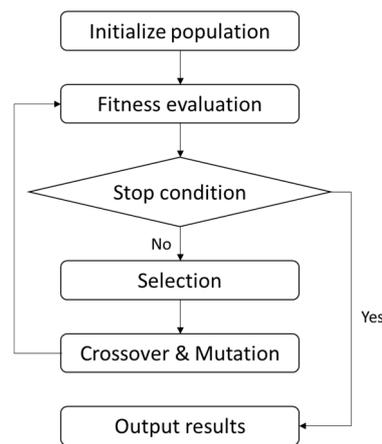
Figure 5. Genetic algorithm procedure.

The implementation of the genetic algorithm starts with the definition of a fixed number of chromosomes, which represent, in this case, one of the possible regression models. At the beginning, chromosomes are encoded and therefore represented in terms of a string of bits, octal numbers, hexadecimal numbers, values, etc. [38]. In this study, real value encoding is adopted, in which every chromosome is represented in terms of a set of real values. The main advantage of this scheme is given by the direct representation of the parameters and by the fact that it avoids any intermediate encoding and decoding steps [32].

In particular, each term of the model:

$$C_i = P^{\alpha_i} \cdot Ss^{\beta_i}, \tag{2}$$

is encoded using two independent genes, i.e., the powers of the variables that constitute each term α_i and β_i, $i = 1, \ldots, N_T$, with α_i, $\beta_i \in Q$, where Q is a discrete set of real values representing all the possible considered exponents for the model. Finally, the coefficients of the regression model (k_i, $i = 0, \ldots, N_T$) are evaluated using a standard linear regression.

The initial population of models is generated by assigning to each gene a random value within the chosen range. The fitness of this population is evaluated by the fitness function, which is built according to the target of the study, thus returning a specific value for the variable of interest:

$$f = \text{rms}(N_{GA}(P_i, Ss_i) - N_E(P_i, Ss_i)), \ i = 1, \ldots, c, \tag{3}$$

where rms represents the root mean square operation, $N_{GA}(P_i, Ss_i)$ is the result obtained by applying the models of the initial population for the specific combination of parameters i, $N_E(P_i, Ss_i)$ is the corresponding experimental measure and c is the number of combinations. The aim of the genetic algorithm is to find the best regression model which minimizes the fit value f.

Then, if the stop condition is not met, the initial population evolves into the next generation through the genetic operators, i.e., selection (i), crossover (ii) and mutation (iii):

i. during new generation, the selection operator decides which chromosomes in the population are transferred to the next one, while eliminating some of them. In this case, the decision is made using the ranking method. In particular, it implies the selection of the individuals by sorting them accordingly to their fitness values (see Equation (3)). Then, the best 50% individuals are chosen to mate, while the remaining 50% are eliminated. In order to maintain a constant number of individuals in the population, 50% new individuals are generated by applying either crossover or mutation operators to the best ones;

ii. the crossover operator increases the variability of the population by letting two random chromosomes, i.e., parents, to exchange genes between themselves, therefore producing a more

powerful individual. Here, the random single-point crossover is considered and applied to every chromosome, as shown in Figure 6;

iii.　the mutation operator is used to avoid local convergence of the genetic algorithm by introducing random variation in the genome of some individuals [32,39]. In fact, while increasing the number of generations, even if the crossover rate is high, chromosomes become more and more similar to each other, therefore blocking diversity and preventing the occurrence of more powerful generations [36]. In particular, the mutation operator only starts after some new generations with a fixed probability of occurrence. As in the case of the crossover, a random single-point mutation is considered (see Figure 7).

Parent 1　　$k_0^1 + k_1^1 \cdot P^{\alpha_1^1} \cdot Ss^{\beta_1^1} + \cdots + k_j^1 \cdot P^{\alpha_j^1} \cdot Ss^{\beta_j^1} + \cdots + k_{N_T}^1 \cdot P^{\alpha_{N_T}^1} \cdot Ss^{\beta_{N_T}^1}$

Parent 2　　$\boldsymbol{k_0^2 + k_1^2 \cdot P^{\alpha_1^2} \cdot Ss^{\beta_1^2} + \cdots + k_j^2 \cdot P^{\alpha_j^2} \cdot Ss^{\beta_j^2} + \cdots + k_{N_T}^2 \cdot P^{\alpha_{N_T}^2} \cdot Ss^{\beta_{N_T}^2}}$

Son　　$k_0^1 + k_1^1 \cdot P^{\alpha_1^1} \cdot Ss^{\beta_1^1} + \cdots + \boldsymbol{k_j^2 \cdot P^{\alpha_j^2} \cdot Ss^{\beta_j^2} + \cdots + k_{N_T}^2 \cdot P^{\alpha_{N_T}^2} \cdot Ss^{\beta_{N_T}^2}}$

Figure 6. Random single-point crossover.

Parent　　$k_0^1 + k_1^1 \cdot P^{\alpha_1^1} \cdot Ss^{\beta_1^1} + \cdots + k_j^1 \cdot P^{\alpha_j^1} \cdot Ss^{\beta_j^1} + \cdots + k_{N_T}^1 \cdot P^{\alpha_{N_T}^1} \cdot Ss^{\beta_{N_T}^1}$

Mutated son　　$k_0^1 + k_1^1 \cdot P^{\alpha_1^1} \cdot Ss^{\beta_1^1} + \cdots + k_j^1 \cdot \boldsymbol{P^{\alpha_j^*}} \cdot Ss^{\beta_j^1} + \cdots + k_{N_T}^1 \cdot P^{\alpha_{N_T}^1} \cdot Ss^{\beta_{N_T}^1}$

Figure 7. Random single-point mutation.

Finally, in order to ensure the global convergence of the algorithm, it is iterated until a defined number of generations in which a stationary fitness value is reached.

3. Results and Discussion

Among the experimental combinations investigated in this research work (see Table 3), it is possible to highlight three main scenarios:

i.　laser treatments carried out at laser power lower than 150 W did not lead to significant changes in the substrates' morphology and any grain structure modification was observed;

ii.　the treatments at 150 and 200 W ensured the best performances. In fact, these process conditions led to a change in substrate properties without melting phenomena, especially with scan speed in the range 16 to 20 mm/s;

iii.　when increasing the laser power to 250 or 300 W, surface melting was observed regardless of the scanning speed.

These results are in good agreement with the pertinent literature [40] and are supported by Figure 8, in which it can be observed that increasing the scan speed by values greater than 14 mm/s, increases the number of cycles until failure, which is almost double the number of cycles obtained with the untreated samples (U label). The improvement in the fatigue life can be attributed to the formation of a superficial annealed martensitic structure due to thermal phenomena induced by the laser treatment [15,25]. In particular, the amount of thermal energy the steel can absorb during the laser treatment decreases, and the process reaches the condition in which it is possible to have the martensitic transition. The subsequent laser scan causes a further heat treatment which leads to a slight annealing of the steel, i.e., back tempering phenomenon [41,42].
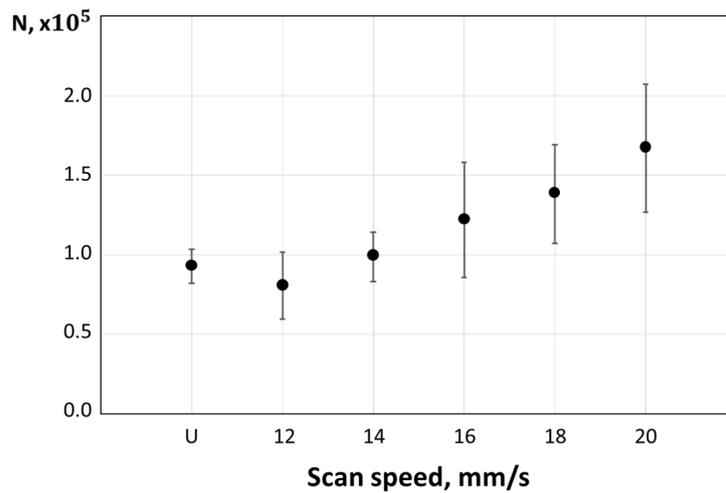
Figure 8. Number of cycles vs. scan speed for a laser power of 200 W. 'U' refers to the untreated samples.

It is worth noting that, during the tests, the coordinate-measuring machine showed no appreciable deformations. In fact, the axial symmetry of the laser treatment helped to compensate for possible distortions.

For sake of clarity, Figure 9 shows a cross section of the steel specimen treated at $P = 200$ W and $Ss = 20$ mm/s. In particular, it can be seen that the martensitic structure, i.e., the light grey area, reaches a thickness of about 182 µm. On the other hand, Table 4 reports the thickness of the martensitic structure, i.e., heat affected zone (HAZ), obtained for some of the investigated values of the scan speed. In particular, when increasing the scan speed the thickness of the martensitic structure increases, according to the fact that, for lower values of the scan speed, the interaction time is greater and the aforementioned back tempering phenomenon takes place.
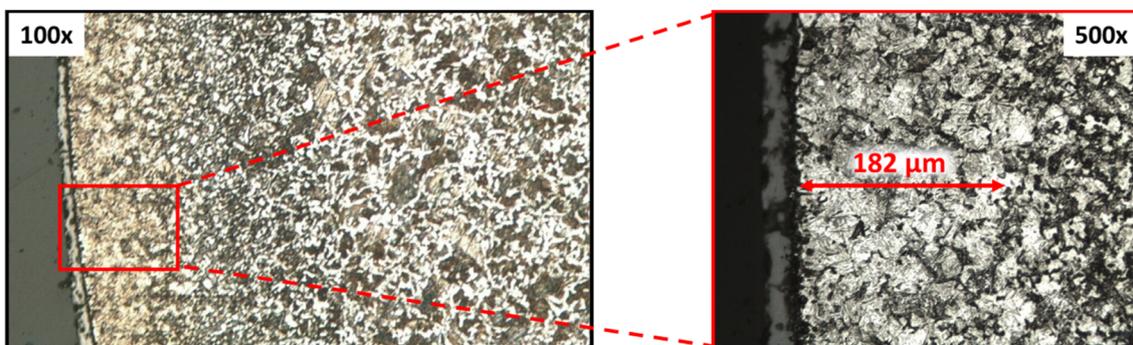

Figure 9. Optical micrography of a laser hardened cross-section: transition from the martensitic structure (light grey) to the ferrite and perlite structure (dark grey) for $P = 200$ W and $Ss = 20$ mm/s.

Table 4. Thickness of the martensitic structure (HAZ) for different values of scan speed.

Ss, mm/s	HAZ, µm
12	67
16	127
20	182

From this experimental campaign it is evident that, among the studied process parameter values, only some combinations allow the effective obtainment of the hardening of the samples (see Table 5). Therefore, only these values are used in the optimization process by means of genetic algorithm, as described in Section 2.1.

Table 5. Combination of parameters (c) used in the optimization process. The 'U' label refers to the untreated samples.

c	Ss, mm/s	P	N
1	18	150	114,754 ± 20,695
2	18	200	224,327 ± 39,017
3	18	250	146,136 ± 18,011
4	20	150	421,982 ± 34,238
5	20	200	364,860 ± 33,197
6	20	250	170949 ± 16,390
U	-	-	92,608 ± 10,698

Among these optimal combinations, the best one is given by P = 150 W and Ss = 20 mm/s leading to an improvement in the fatigue life more than 4 times that of the untreated samples, i.e., 421,982 against 92,608 cycles until failure, as reported in Table 5.

It is important to highlight here that the laser treatments were carried out in order to maintain a constant scan speed. To this end, the rotating speed of the sample was changed according to the varying section when moving from the largest section zone to the smallest one. Moreover, all the parameters were chosen to avoid, or at least limit, the overlapping phenomenon. This means that the interaction time between the laser beam and the specimen is different at the various scan speeds investigated. In particular, the lower the scan speed, the higher the interaction time. It is worth mentioning that, as reported in the literature [42,43], the interaction time is suggested to be proportional to the laser power. Therefore, increasing the laser power over 250 W, the heat transferred to the sample is greater and the melting phenomena occurs. On the other hand, a laser power that is too low, i.e., 100 W, in combination with the investigated scan speed values, does not promote the martensitic transition, as it happens for too high and too short a treatment time, respectively.

Genetic Algorithm-Based Optimization

The aim of this step is to find the best regression model able to fit the experimental data among the infinite possible combinations of input parameters and their powers in terms of the number of cycles until failure (N_{GA}), as reported in Equation (1).

A preliminary investigation aimed at identifying the best number of terms for the optimized regression model. To this end, the number of terms was increased starting from two, i.e., one term plus the constant one, to the number of terms after which any more decrease in the fitness value is obtained. Additionally, three different discrete sets of real values representing all the possible exponents were investigated (see Table 6). In this way, the explored space is discrete and contains the number of exponents to the power of $N_T \cdot N_V$ possible models, where N_V is the number of variables constituting each term (2 in this case).

Table 6. Discrete set of real values representing the possible exponents.

Set	Exponents
Q_1	{0, 1, 2}
Q_2	{−2, −1, 0, 1, 2}
Q_3	{−2, −1, −0.5, 0, 0.5, 1, 2}

Moreover, in order to evaluate the capability of the optimized models in representing the experimental findings, they were compared with the regression model typically used for statistical investigations, as in the case of two-way ANOVA test, i.e., considering the effect of each single

parameter and their combinations [44]. In this case, the set of possible exponents Q_R can be defined as $\{0, 1\}$, while the statistical regression model is described by the following equation:

$$N_R = k_0 + k_1 \cdot Ss + k_2 \cdot P + k_3 \cdot Ss \cdot P. \tag{4}$$

Figure 10 shows the results obtained during the preliminary investigation. In particular, among the different combinations of numbers of terms and sets of exponents, the worst one, i.e., the one with the highest fitness value, is the model with only two terms, as expected. While the best models were obtained with four terms, adding more terms did not lead to a decrease in the fitness value. It is important to note that, for the regression model, the number of terms is set at four, which is the number of possible combinations. The resulting optimized models are described by Equations (5)–(7), while Table 7 reports the relative empirical coefficients, evaluated by means of standard linear regression.

$$N_{GA}^1 = k_0^1 + k_1^1 \cdot P + k_2^1 \cdot Ss^2 + k_3^1 \cdot Ss^2 \cdot P^2 \tag{5}$$

$$N_{GA}^2 = k_0^2 + k_1^2 \cdot \frac{1}{Ss \cdot P^2} + k_2^2 \cdot \frac{Ss^2}{P} + k_3^2 \cdot Ss^2 \cdot P \tag{6}$$

$$N_{GA}^3 = k_0^3 + k_1^3 \cdot \frac{1}{Ss \cdot P} + k_2^3 \cdot \frac{Ss}{\sqrt{P}} + k_3^3 \cdot Ss \cdot \sqrt{P} \tag{7}$$
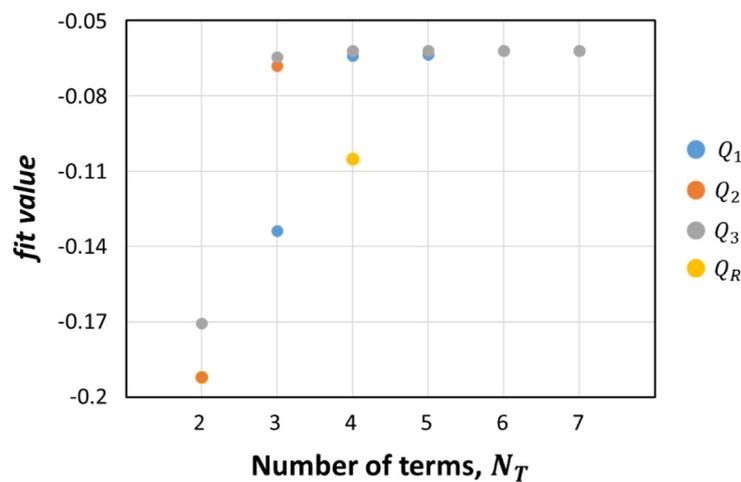

Figure 10. Fitness value for different number of terms.

Table 7. Empirical coefficients of the genetic algorithm-optimized models.

Coefficients *	Set		
	Q_1	Q_2	Q_3
k_0^i	−6.420	1.587	8.314
k_1^i	6.628	−0.959	−4.016
k_2^i	5.147	2.019	4.539
k_3^i	−4.993	−2.271	−8.462

*: $i = 1, 2, 3$ refers to the investigated sets of exponents Q_i.

As shown in Figure 10, the statistical model is characterized by a fitness value greater, yet more negative, than the optimal value obtained with the genetic algorithm, i.e., −0.1052 against −0.0622. In order to better clarify this result, Figure 11 shows the root mean square error and the standard deviation of the regression models compared with the experimental findings for each combination of parameters (see Table 5).
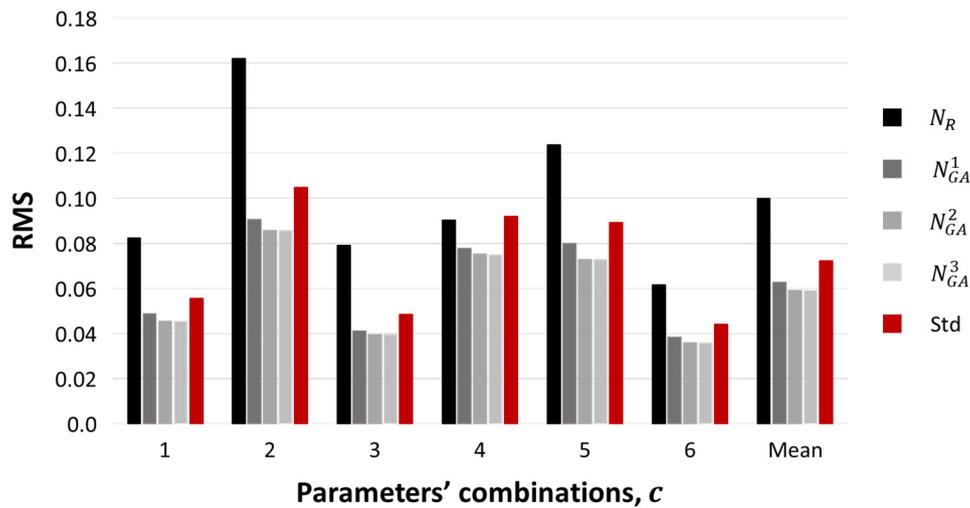
Figure 11. Comparison of the root mean square error for each combination of parameters between the optimized models, the statistical model and the standard deviation of the experimental data.

As shown in Figure 11, the genetic algorithm-optimized models are able to accurately replicate the experimental results with an error almost half that of the mean error obtained with the statistical model, i.e., 0.0603 against 0.0998. Moreover, these models are characterized by a mean error comparable to and even lower than the standard deviation of the experimental data, i.e., 0.0603 against 0.0723, which is associated with the variability of the process, highlighting the good capability of the model to replicate the experimental trend. It is worth noting that the best optimized model is given by using the set of exponents Q_3 (see Table 6), for which the mean error is about 0.0591. For completeness, Figure 12 shows the optimal model results.
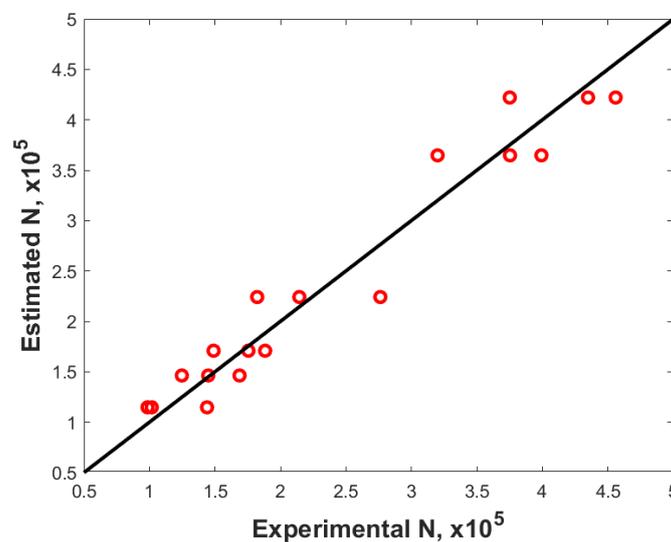

Figure 12. Optimal genetic algorithm (GA)-based model results.

In general, convergence was reached in less than 15 generations, as shown in Figure 13. In each generation, 1000 individuals (i.e., models) were evaluated. In practice, the GA explores a space of cardinality $C \cong 5.7 \cdot 10^6$ solving only $1.5 \cdot 10^4$ models. A further 50 generations were computed to verify if mutation can move the optimum from a local minimum toward a better solution. The optimization algorithm was run several times, always obtaining the same result, ensuring in this way that the GA reached a global minimum.
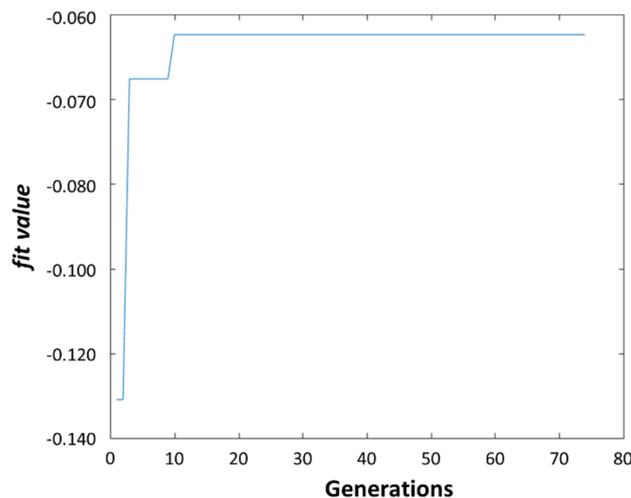
Figure 13. Number of generations before convergence.

4. Conclusions

The 1.5 kW continuous wave high-power diode laser used in this study demonstrated a high suitability for the surface hardening of AISI 1040 medium carbon steel substrates.

The inspection of the cross-sections of the specimens by means of optical microscopy revealed two different main areas: (i) an outer area characterized by a homogenous distribution of the annealed martensite and (ii) an unaltered underling area made of a ferrite and perlite structure.

The laser thermal surface treatment increases the fatigue life of the treated material with respect to the untreated one. In particular, within the tested range of the parameters, the most suitable thermal conditions are obtained using a laser power of 150 W and a scan speed of 20 mm/s, reaching a fatigue life up to four times longer.

The proposed genetic algorithm-based method appeared to be a fast and effective solution for finding the optimal regression model able to replicate the experimental trend. In particular, the mean error achieved is about 5.9%, the same as the standard deviation of the experimental results. Therefore, the simulation reveals a good capability for the proposed solutions to be very helpful in predicting, controlling and managing the laser surface hardening process.

Author Contributions: Conceptualization, S.G.; methodology, S.G. and G.S.P., software, O.G. and G.S.P.; validation, G.S.P.; formal analysis, O.G., S.G. and G.S.P.; investigation, S.G.; writing—original draft, G.S.P.; writing—review & editing, O.G., S.G. and G.S.P. All authors have read and agreed to the published version of the manuscript.

References

1. Santos, L.M.S.; Ferreira, J.A.M.; Jesus, J.S.; Costa, J.M.; Capela, C. Fatigue behaviour of selective laser melting steel components. *Theor. Appl. Fract. Mech.* **2016**, *85*, 9–15. [CrossRef]
2. Yıldırım, H.C. Recent results on fatigue strength improvement of high-strength steel welded joints. *Int. J. Fatigue* **2017**, *101*, 408–420. [CrossRef]
3. Maharjan, N.; Zhou, W.; Zhou, Y.; Guan, Y.; Wu, N. Comparative study of laser surface hardening of 50CrMo4 steel using continuous-wave laser and pulsed lasers with ms, ns, ps and fs pulse duration. *Surf. Coat. Technol.* **2019**, *366*, 311–320. [CrossRef]
4. Nath, A.K.; Sarkar, S. Laser Transformation Hardening of Steel. In *Advances in Laser Materials Processing*; Elsevier: Cambridge, UK, 2018; pp. 257–298. ISBN 9780081012529.

5. Vollertsen, F.; Partes, K.; Meijer, J. State of the Art of Laser Hardening and Cladding. In Proceedings of the Third International WLT-Conference Lasers Manufacturing, Munich, Germany, 13–16 June 2005.

6. Lakhkar, R.S.; Shin, Y.C.; Krane, M.J.M. Predictive modeling of multi-track laser hardening of AISI 4140 steel. *Mater. Sci. Eng. A* **2008**, *480*, 209–217. [CrossRef]

7. Jiang, J.; Xue, L.; Wang, S. Discrete laser spot transformation hardening of AISI O1 tool steel using pulsed Nd:YAG laser. *Surf. Coat. Technol.* **2011**, *205*, 5156–5164. [CrossRef]

8. Khorram, A.; Davoodi Jamaloei, A.; Jafari, A.; Moradi, M. Nd:YAG laser surface hardening of AISI 431 stainless steel; mechanical and metallurgical investigation. *Opt. Laser Technol.* **2019**, *119*, 105617. [CrossRef]

9. Nath, A.K.; Gupta, A.; Benny, F. Theoretical and experimental study on laser surface hardening by repetitive laser pulses. *Surf. Coat. Technol.* **2012**, *206*, 2602–2615. [CrossRef]

10. Sancho, P.; Montealegre, M.A.; Dominguez, J.; Alvarez, P.; Isaza, J. Dynamic control of laser beam shape for heat treatment. *J. Laser Appl.* **2018**, *30*, 032507. [CrossRef]

11. Moradi, M.; Arabi, H.; Karami Moghadam, M.; Benyounis, K.Y. Enhancement of surface hardness and metallurgical properties of AISI 410 by laser hardening process; diode and Nd:YAG lasers. *Optik* **2019**, *188*, 277–286. [CrossRef]

12. Filep, A.; Benke, M.; Mertinger, V.; Buza, G. Residual Stress Distribution Caused by Laser Hardening and Conventional Quenching in Plain Carbon Steel. *Adv. Mater. Res.* **2014**, *996*, 538–543. [CrossRef]

13. Liverani, E.; Lutey, A.H.A.; Ascari, A.; Fortunato, A.; Tomesani, L. A complete residual stress model for laser surface hardening of complex medium carbon steel components. *Surf. Coat. Technol.* **2016**, *302*, 100–106. [CrossRef]

14. Pashby, I.R.; Barnes, S.; Bryden, B.G. Surface hardening of steel using a high power diode laser. *J. Mater. Process. Technol.* **2003**, *139*, 585–588. [CrossRef]

15. Liu, A.; Previtali, B. Laser surface treatment of grey cast iron by high power diode laser. *Phys. Procedia* **2010**, *5*, 439–448. [CrossRef]

16. Lambiase, F.; Di Ilio, A.M.; Paoletti, A. Prediction of Laser Hardening by Means of Neural Network. *Procedia CIRP* **2013**, *12*, 181–186. [CrossRef]

17. Skvarenina, S.; Shin, Y.C. Predictive modeling and experimental results for laser hardening of AISI 1536 steel with complex geometric features by a high power diode laser. *Surf. Coat. Technol.* **2006**, *201*, 2256–2269. [CrossRef]

18. Ion, J.C. Laser Transformation Hardening. *Surf. Eng.* **2002**, *18*, 14–31. [CrossRef]

19. Moradi, M.; KaramiMoghadam, M. High power diode laser surface hardening of AISI 4130; statistical modelling and optimization. *Opt. Laser Technol.* **2019**, *111*, 554–570. [CrossRef]

20. Anusha, E.; Kumar, A.; Shariff, S. Diode Laser Surface Treatment of Bearing Steel for Improved Sliding Wear Performance. *Optik* **2019**, 163357. [CrossRef]

21. Oh, S.; Ki, H. Prediction of hardness and deformation using a 3-D thermal analysis in laser hardening of AISI H13 tool steel. *Appl. Therm. Eng.* **2017**, *121*, 951–962. [CrossRef]

22. Liverani, E.; Sorgente, D.; Ascari, A.; Scintilla, L.D.; Palumbo, G.; Fortunato, A. Development of a model for the simulation of laser surface heat treatments with use of a physical simulator. *J. Manuf. Process.* **2017**, *26*, 262–268. [CrossRef]

23. Guarino, S.; Ponticelli, G.S. High Power Diode Laser (HPDL) for Fatigue Life Improvement of Steel: Numerical Modelling. *Metals* **2017**, *7*, 447. [CrossRef]

24. Rao, R.V. *Decision Making in the Manufacturing Environment: Using Graph Theory and Fuzzy Multiple Attribute Decision Making Methods*; Springer: London, UK, 2007; ISBN 9781849966535.

25. Kennedy, E.; Byrne, G.; Collins, D.N. A review of the use of high power diode lasers in surface hardening. *J. Mater. Process. Technol.* **2004**, *155–156*, 1855–1860. [CrossRef]

26. Guarino, S.; Barletta, M.; Afilal, A. High Power Diode Laser (HPDL) surface hardening of low carbon steel: Fatigue life improvement analysis. *J. Manuf. Process.* **2017**, *28*, 266–271. [CrossRef]

27. Bauccio, M. *ASM Metals Reference Book*, 3rd ed.; ASM International: Russell Township, OH, USA, 1993; ISBN 9780871704788.

28. Shin, H.J.; Yoo, Y.T.; Ahn, D.G.; Im, K. Laser surface hardening of S45C medium carbon steel using ND:YAG laser with a continuous wave. *J. Mater. Process. Technol.* **2007**, *187–188*, 467–470. [CrossRef]

29. Goia, F.A.; De Lima, M.S.F. Surface hardening of an AISI D6 cold work steel using a fiber laser. *J. ASTM Int.* **2011**, *8*, 103210. [CrossRef]

30. Parida, B.K. Fatigue Testing. In *Encyclopedia of Materials: Science and Technology*; Elsevier: London, UK, 2001; pp. 2994–2999.

31. Sarkar, A.; Okazaki, M.; Nagesha, A.; Parameswaran, P.; Sandhya, R.; Laha, K. Mechanisms of failure under low cycle fatigue, high cycle fatigue and creep interactions in combined cycling in a type 316LN stainless steel. *Mater. Sci. Eng. A* **2017**, *683*, 24–36. [CrossRef]

32. Verotti, M.; Di Giamberardino, P.; Belfiore, N.P.; Giannini, O. A genetic algorithm-based method for the mechanical characterization of biosamples using a MEMS microgripper: Numerical simulations. *J. Mech. Behav. Biomed. Mater.* **2019**, *96*, 88–95. [CrossRef]

33. Dumont-Fillon, D.; Hannebelle, M.; Van Lintel, H.; Chappel, E. Design of a Passive Flow Regulator Using a Genetic Algorithm. *Procedia Eng.* **2016**, *168*, 1016–1019. [CrossRef]

34. Alberdi, R.; Khandelwal, K. Comparison of robustness of metaheuristic algorithms for steel frame optimization. *Eng. Struct.* **2015**, *102*, 40–60. [CrossRef]

35. Ponticelli, G.S.; Guarino, S.; Tagliaferri, V.; Giannini, O. An optimized fuzzy-genetic algorithm for metal foam manufacturing process control. *Int. J. Adv. Manuf. Technol.* **2019**, *101*, 603–614. [CrossRef]

36. Dao, S.D.; Abhary, K.; Marian, R. A bibliometric analysis of Genetic Algorithms throughout the history. *Comput. Ind. Eng.* **2017**, *110*, 395–403. [CrossRef]

37. Aguirre, H.; Tanaka, K.; Aguirre, H.; Tanaka, K. A Model for Parallel Operators in Genetic Algorithms. In *Parallel Evolutionary Computations*; Springer: Berlin/Heidelberg, Germany, 2006; pp. 3–31.

38. Kumar, A. Encoding schemes in genetic algorithm. *Int. J. Adv. Res. IT Eng.* **2013**, *3*, 1–7.

39. Esen, İ.; Koç, M.A. Optimization of a passive vibration absorber for a barrel using the genetic algorithm. *Expert Syst. Appl.* **2015**, *42*, 894–905. [CrossRef]

40. Lusquiños, F.; Conde, J.C.; Bonss, S.; Riveiro, A.; Quintero, F.; Comesaña, R.; Pou, J. Theoretical and experimental analysis of high power diode laser (HPDL) hardening of AISI 1045 steel. *Appl. Surf. Sci.* **2007**, *254*, 948–954. [CrossRef]

41. Gisario, A.; Barletta, M.; Boschetto, A. Characterization of laser treated steels using instrumented indentation by cylindrical flat punch. *Surf. Coat. Technol.* **2008**, *202*, 2557–2569. [CrossRef]

42. Gisario, A.; Barletta, M.; Conti, C.; Guarino, S. Springback control in sheet metal bending by laser-assisted bending: Experimental analysis, empirical and neural network modelling. *Opt. Lasers Eng.* **2011**. [CrossRef]

43. Vilar, R. Laser surface modification of steel and cast iron for corrosion resistance. In *Laser Surface Modification of Alloys for Corrosion and Erosion Resistance*; Elsevier: Cambridge, UK, 2012; pp. 3–40. ISBN 9780857090157.

44. Miller, R.G.; Brown, B.W. *Beyond ANOVA: Basics of Applied Statistics*; Chapman & Hall: London, UK, 1997; ISBN 9780412070112.